J. Fluid Mech. (1985), *vol.* 157, *pp.* 35–51
Printed in Great Britain

Experiments on fluid flow induced by melting around a migrating heat source

By M. K. MOALLEMI AND R. VISKANTA
School of Mechanical Engineering, Purdue University, West Lafayette, IN 47907, U.S.A.

(Received 17 February 1984 and in revised form 7 January 1985)

A series of melting experiments with a moving horizontal cylindrical heat source at constant surface heat flux have been performed. The heat source was designed in such a way that it could descend under its weight while melting the phase-change material (*n*-octadecane) surrounding it. The heat-source velocity was measured and the motion and shape of the solid–liquid interface were determined photographically. The effects of the surface heat flux, the density and initial position of the heat source, and the initial subcooling of the solid were investigated and are discussed. Conduction was found to be the dominant heat-transfer mechanism around the lower stagnation point and controlled the terminal velocity of the source. The fluid motion in the melt pool above the heat source was mainly induced by the descent of the source, while natural convection played only a relatively minor role in the motion.

1. Introduction

The problem of melting in the vicinity of a moving heat source arises in many different physical situations in such diverse fields as materials processing (Jackson 1965), spacecraft and nuclear technology (Tong 1968) and geology (Marsh & Charmichael 1974). In the field of nuclear technology, this problem has two important applications. One application is the 'self-burial' process, a nuclear-waste-disposal scheme which suggests placing the radioactive waste materials in various cavities in the ground (Cohen, Schwartz & Tewes 1974) or on the Arctic ice cap (Herrmann 1983). Another application is the reactor core 'melt-down' accident also referred as the China syndrome (Jansen & Stepnewski 1973; and Rasmussen *et al.* 1979). In geophysics, applications include magma migration (Marsh 1978) and core formation (Christoffel & Calhaen 1973).

If a heat source releases heat in excess of a certain minimum that its surroundings can conduct, the surroundings will eventually melt and the heat source will start moving in the liquid melt in the direction of the net force exerted on it (gravitational, buoyancy, shear forces, etc.). The problem considered here is a combination of two important classes of heat-transfer problems, those involving phase change and those with a moving heat source. The combination of these two phenomena introduces processes which do not exist in either case alone. These include development of a film flow between the heat source and the solid due to motion of the heat source, development of a mixed convection flow in the melt, and solidification of the melt after passage of the heat source.

None of these processes has received attention in the limited number of studies presently available in the literature. Regardless of the fact that the published analyses are approximate, they are not based on realistic physical models of the processes involved. Important phenomena such as phase change (Easton 1968 and

Donea 1972) and natural and forced convection (Hardee & Sullivan 1973, 1974 and Logan 1974) have been neglected. Less important processes such as resolidification of the melt have also been ignored. A more realistic model has recently been suggested by Emerman & Turcotte (1983). The migration velocity of a hot rigid sphere which melts its way through a solid was calculated but the processes which occur in the molten wake behind the sphere were ignored and the solution is only valid as long as the hot sphere and the solid are separated by a very thin melt layer. Experiments are even more scarce (Armstrong *et al.* 1965; Robinson *et al.* 1971; and Donea 1972) and can be categorized as feasibility or assessment studies rather than phenomenological or parametric studies.

The objective of this investigation is to report on the important heat-transfer and fluid-flow processes during melting around a moving heat source and the extent and range of their effects. Experiments have been performed by employing a horizontal cylindrical heat source with a constant surface heat flux which melted its way through the phase-change material and descended under its own weight. The phase-change material used in the experiments was research grade (99.9% pure) *n*-octadecane paraffin, as its liquid phase is transparent and permits flow visualization and photography. Its properties are well documented and its fusion temperature is close to room temperature (27.5 °C), which is conducive to experimentation.

The work included two groups of experiments. In the first group the heat source was initially placed on top of the solid. A supplementary set of experiments was performed in which the heat source was initially embedded in the solid matrix. In addition to this, three other parameters were varied during the course of the study, namely surface heat flux of the heat source, initial temperature of the solid, and the apparent weight of the heat source. The report includes measurements and/or observations of the heat-source velocity, the shape and motion of the solid–liquid interface and characteristics of the temperature and the flow fields in the melt.

2. Experiments

2.1. *Apparatus and instrumentation*

The experiments were performed in a test cell having a rectangular cross-section of 35.5 × 7.5 cm and 25.5 cm depth (figure 1). The test cell consists of a main U-shaped aluminium frame (1), 7.4 cm thick, attached to a horizontal rectangular base plate on four adjustable levelling screws. The front and back sides of the cell are made of 0.6 cm thick glass plate to allow visualization and photographing. To ensure two-dimensionality a second glass plate was installed on each side, parallel to the first one, to reduce the overall heat transfer between the test cell and the ambient environment. The top of the test cell was closed before and during the experiments with a Plexiglas cover plate (2). Two parallel bushings (5) were fixed to the Plexiglas cover plate which guided the heat-source support tubes (8.2 mm o.d.) in the vertical direction and prevented the heat source from tilting or rotating during its migration.

The apparent weight of the heat source (the net force exerted by the heat source to the melt and/or solid) is one of the governing parameters of the problem and provisions were made to change and control it. The apparent weight was increased by adding weight to the support tubes and was decreased by adding counterbalance weight (by using a pair of pulleys). The apparent weight of the heat source was measured under test conditions (velocity of the heat source was of the same order of magnitude as was estimated for a melting experiment) to compensate for frictional force between the support tubes and the bushing guides.

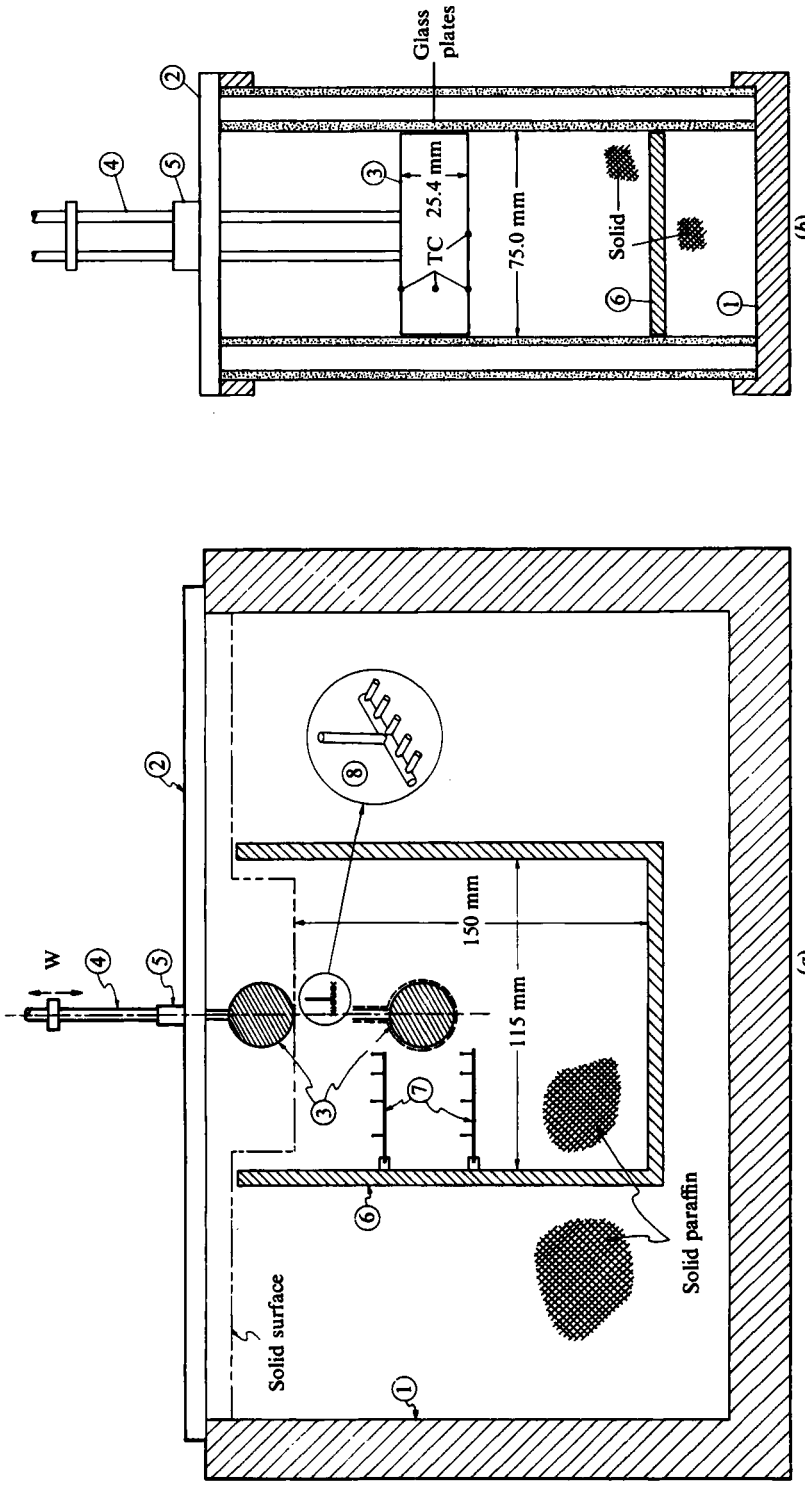

FIGURE 1. Schematic diagram of the setup, (*a*) front view and (*b*) side view: (1) main frame of the test cell, (2) Plexiglas cover, (3) heat source (two starting positions), (4) support tubes, (5) guide bushings, (6) U-shaped heat exchanger, (7) thermocouples positioned in solid, (8) thermocouples positioned in melt.

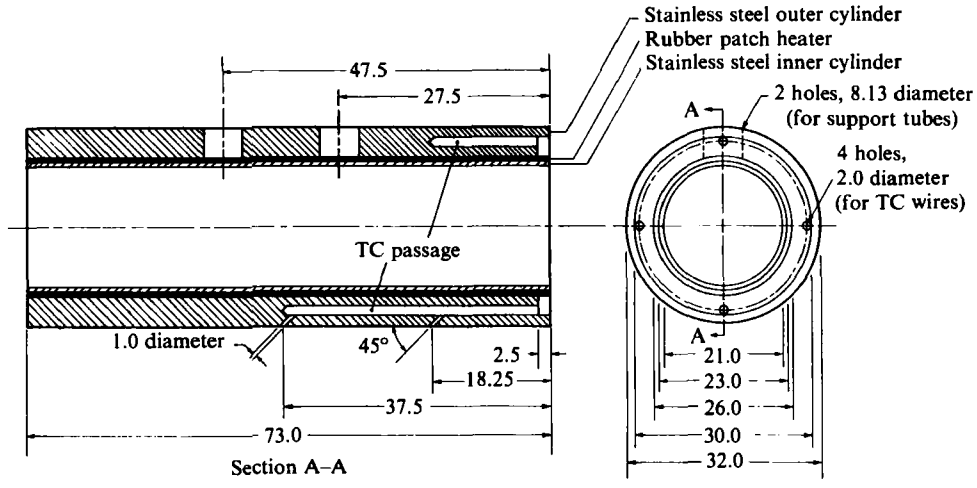

FIGURE 2. Schematic diagram of the constant surface-heat-flux heat source, all dimensions in mm.

The solid temperature was controlled by a U-shaped multipass heat exchanger (6) which was placed inside the test cell before pouring in the liquid. The heat exchanger was connected to a constant-temperature bath for several hours before and also during the experiments in order to maintain the test cell and the solid at a preselected temperature (at or below the melting point of the phase-change material). To check the uniformity of the temperature throughout the solid before starting an experiment and also to measure the temperatures in the solid during the test (for subcooled-solid cases), a total of sixteen thermocouples (7) were located at fixed positions in the test cell. The temperature distribution in the melt was measured by five thermocouples installed on a T-shaped probe (8) which was placed in the melt after the passage of the heat source.

A circular cylindrical ($L/R = 4.8$) heat source was designed and built to provide constant surface heat flux (figure 2). The extremely non-uniform external thermal conditions and the two-dimensionality of the heat source were major design constraints. A constant-heat-generating electrical patch heater was tightly fitted between two thin-walled stainless-steel cylindrical shells. Seven thermocouples were placed on the heat-source surface (at $\frac{1}{4}L$, and $\phi = 0, 90, 180$ and $270°$; at $\frac{1}{2}L$ and $\phi = 0$, 90 and $270°$) for measuring the temperature distribution on the heat source. The thermocouple wires and the electrical power leads of the heater were passed through the support tubes to minimize their interference with the flow field. Two end caps (1.0 mm thick) were used to seal the heat source. Heat which is generated uniformly is transferred to a thin wall of low-thermal-conductivity material (stainless steel). Under normal conditions little heat is expected to be transferred in the circumferential direction.

The patch heater (figure 2) was of an irregular pattern of very thin wire sandwiched between two thin sheets of rubber (total thickness of 1.2 mm, manufactured by Electrofilm, Inc.). It had a maximum rated flux of 15000 W/m^2 at 115 volts and was bent and glued around the inner cylindrical shell. This was then tightly fitted in the outer shell. An outer diameter of the inner cylinder was chosen such that the distance between the two ends of the patch heater after bending (on top of the shell) was only 2 mm to allow the electric leads and the thermocouple wires to pass through the support tubes. This resulted in a small unheated strip along the top of the heat source.

A variable transformer and a wattmeter (with a resolution 0.5 W) were used to control and measure the output of the heat source.

The copper–constantan thermocouples on the heat source, throughout the solid and the ones to be placed in the melt pool were connected to an Esterline Angus (Model PD-2064) programmable data-acquisition system for temperature measurement. The system was equipped with a printer and an option to provide for thermocouple linearization and cold-junction compensation. It has an overall accuracy of ± 0.5 °C which was improved to ± 0.2 °C (with 90% confidence) by calibration. The data-acquisition system was also equipped with an option to trigger a camera at the same instant that the temperatures were being measured and recorded.

A transparent sheet marked with grid lines 10 mm apart was attached to the front glass plate to serve as a scale. The relative position of the centre of the heat source and the temperatures were measured at the same time, with a cathetometer with 0.05 mm resolution.

2.2. *Experimental procedure*

To prevent void formation during freezing the paraffin was always degasified before each experiment. The paraffin was first heated in a vacuum flask well above its fusion temperature (to about 150 °C). The flask was then connected to a vacuum pump while being cooled very slowly to about 30 °C (2 °C above the fusion temperature). The paraffin was then syphoned into the test cell. A constant-temperature bath set at 10 °C was then connected to the U-shaped heat exchanger to facilitate freezing.

During freezing formation of internal voids associated with the contraction which accompanies freezing was avoided by preventing the formation of a frozen crust at the upper surface of the paraffin while the liquid phase still existed underneath. This was accomplished by freezing the paraffin from the bottom up. To do this the upper surface was irradiated with an intensity-controlled heat lamp while the bottom and sides were cooled by the U-shaped heat exchanger. Degasified liquid was added several times during solidification to compensate for the contraction. In spite of this, the final upper surface was not flat and levelling was necessary particularly when the melting was to start from the top. Thus, the liquid was frozen to a height about 10 mm above the planned final height. The additional solid was then melted by a hot steel plate which could only move in the vertical direction. The melted material was immediately removed by a hand pump to avoid refreezing.

Once the freezing and the levelling was completed, the constant-temperature bath connected to the U-shaped heat exchanger was set at a preselected value of the solid initial temperature, either the melting point (27.5 °C) or subcooled to 21 °C or 10 °C. For the first of these cases, solid was actually subcooled for a few tenths of a degree below the melting point to avoid melting the impurities. Measured solid temperatures were used to check the uniformity of the temperature field in the solid. These measurements showed that a 10 h period was sufficient for the equilibration.

Four different values for the heat-source input power were employed, 10, 20, 40 and 80 W, for each of the solid initial temperatures. These correspond, respectively, to surface heat fluxes of 1315, 2630, 5260 and 10520 W/m^2 of the heat source, ends excluded.

A coloured wax, commercially used for making candles, was used to visualize the flow patterns in the melt pool above the heat source. It was introduced very slowly and carefully in small quantities by a syringe about midway between the front glass wall and the first support tube. The composition of the coloured wax was not known, but as it was slightly denser than *n*-octadecane it was diluted at a ratio of 1 to 5.

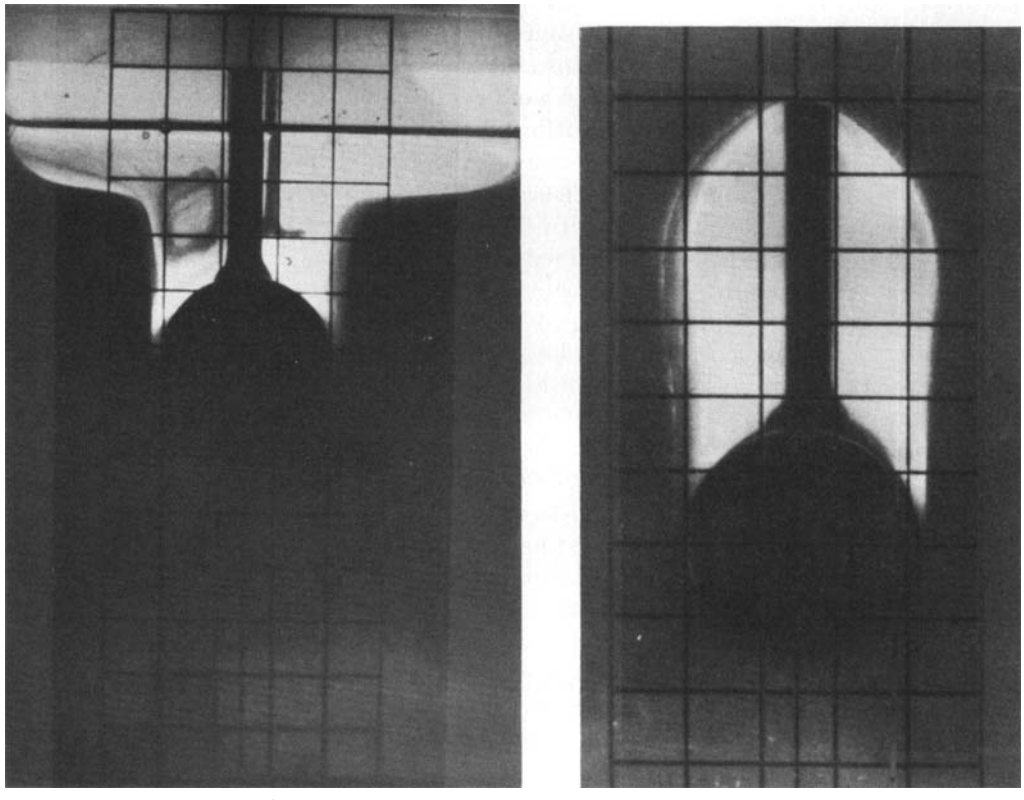

(a) (b)

FIGURE 3. Photographs illustrating the heat source and the solid–liquid interface position: (a) heat source initially on the top of solid; (b) heat source initially in the solid.

3. Results and discussion

3.1. *General observations and phenomena*

The following generalizations are true for both starting positions of the heat source (i.e. at the top of the solid or initially embedded in the solid), and the exceptions will be clearly identified. Figure 3 shows typical photographs of the instantaneous heat source and the solid–liquid interface positions. The heat source is almost in contact with the solid in the vicinity of its lower stagnation point ($\phi = 0°$). The thickness of the thin melt film separating the source and the solid increases with ϕ, and eventually the solid and the heat source become distinguishable at $\phi < 90°$. Careful examination of the photographs revealed that the angular position of this film separation point decreases with increasing heat flux imposed at the heat-source surface and also with an increase in the initial temperature of the solid.

Thin-film separation at the stagnation point and the fact that this film widens with ϕ suggests that the motion of the heat source is essentially defined by the motion of the solid–liquid interface at $\phi = 0°$. Moreover, conduction is the sole mode of heat transfer between the heat source and the solid in this region. As ϕ increases, less material is melted for the same amount of heat generated by the patch heater. Also, the thermal resistance of the film increases with its thickness (i.e. with ϕ). This results in an increase of the melt bulk temperature as well as the heat-source surface

temperature. In addition, the mass flux of the melt also increases along the melt-film channel. All of these factors suggest that a transition from conduction- to convection-dominated melting will occur along the film channel.

For $\phi > 90°$, convection between the melt and the solid is the dominant heat-transfer mechanism which dictates the motion and shape of the solid–liquid interface. Figures 4(*a*), (*b*) and (*c*) illustrate the flow patterns around the heat source inferred from the dye-visualization experiments for different subcoolings of the solid and initial heat-source positions. The newly melted material is squeezed between the solid and the heat source by the descent of the source and moves along the source surface as the film channel widens. The motion of the heat source generates a region of low pressure behind it and causes the new melted material to maintain its direction and move parallel to the heat-source surface. The two streams of the melt, coming from either side of the cylinder, meet at about the centreline and the fluid can only flow upward. At the same time, the melt close to the heat source is heated and also aided by buoyancy in the upward motion. After reaching the free surface (figures 4*a* and *b*) or the solid ceiling for the experiment when the heat source is initially embedded in solid (figure 4*c*), the melt stream is divided into two equal currents and moves along the free surface (or along the solid ceiling). The melt loses some of the heat to the air above it and/or to the solid while flowing sideways. Depending on the solid temperature and also on the melt temperature (which is obviously a function of the heat flux at the surface), some melting and/or resolidification takes place at the solid–liquid interface (compare figures 4*a* and *b*). The melt also loses momentum due to the shear at the solid surface while being cooled and becoming denser. This causes a downward motion of the melt along the vertical solid–liquid interface. Heat transfer between the melt and the solid may result in some resolidification or further melting of the solid, depending on the initial temperature of the solid.

The descending melt stream eventually meets the newly formed melt being squeezed out of the gap between the solid and the falling heat source and is forced to turn parallel to it in an inner path. The curvature of the interface either changes sign or goes through a sudden change in the vicinity of this point (more clearly for the embedded case). This confirms the fact that the two streams interact differently with the solid owing to the large difference in their temperatures and momentum near this location, and there is little mixing of the two streams. The newly melted material follows the path already explained while pushing the cooler, slower melt into a smaller inner loop which is gradually decelerated and creates a region of stagnant melt.

In the flow-visualization experiments, when the dye was introduced on the free surface on one side of the centreline, very little melt (if any at all) reached the other side of the centre line. After some time the melt with the dye was partly resolidified on the edges of the solid (for initially subcooled solid only) and partly concentrated in the nearly stagnant central core. The two similar and independent melt cells on the sides of the vertical plane of symmetry only elongated as the heat source descended and new melt was introduced. The melt cells are essentially two-dimensional. The dye which was introduced at quarter or half way between the glass walls did not move along the axis of the cylinder. Viewed from the top, the dyed melt loop had the appearance of a narrow strip diffusing very slowly in the direction of the axis of the source.

The instantaneous positions of the solid–liquid interface at different times were recorded photographically. A typical time series of photographs was used to plot the instantaneous position of the solid–liquid interface relative to the moving heat source

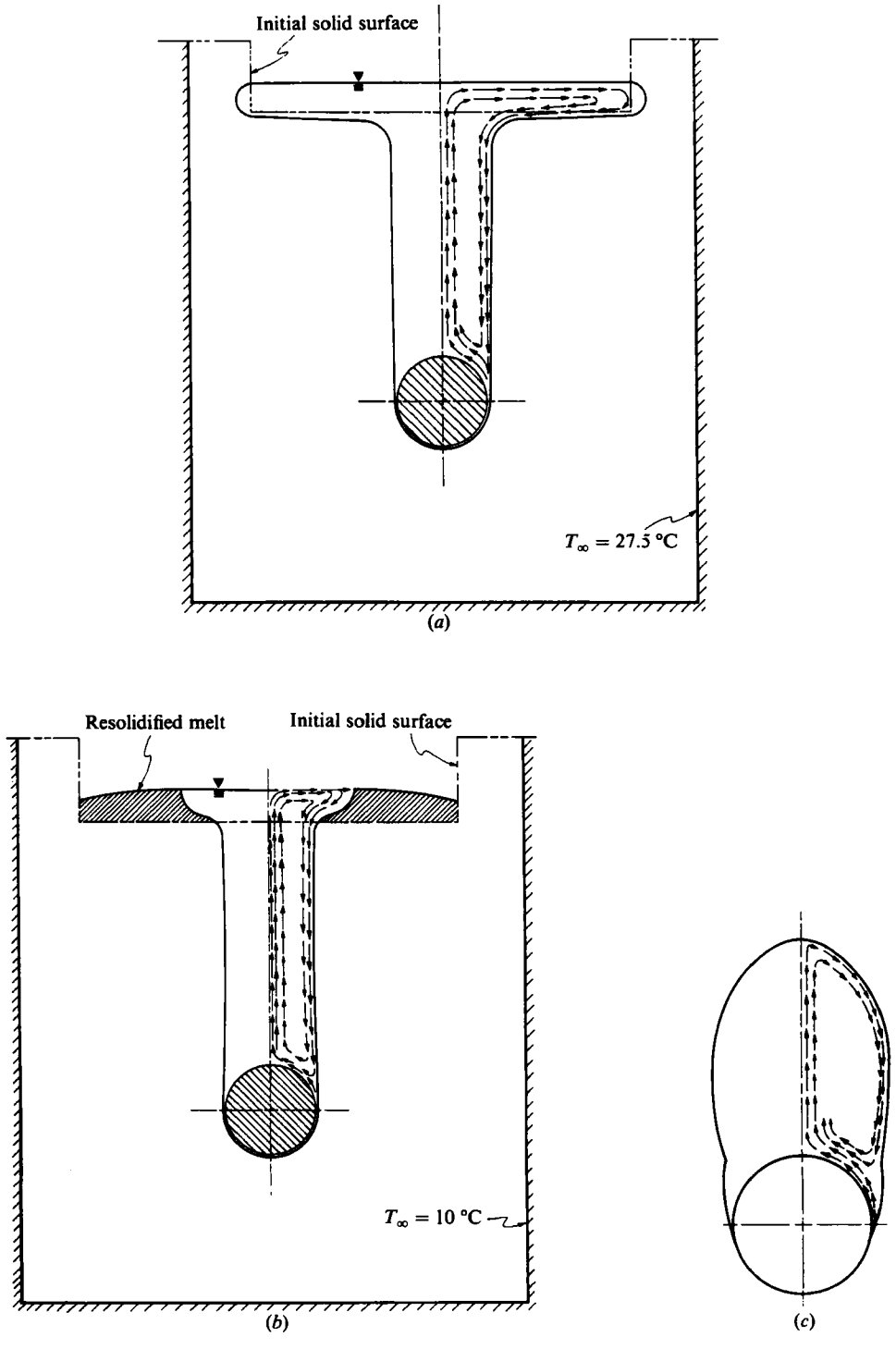

FIGURE 4. The interface shape and melt flow pattern: (*a*) $T_m - T_\infty = 0.5°$; (*b*) 18.0°; (*c*) 7.5°, for the embedded-heat-source case.

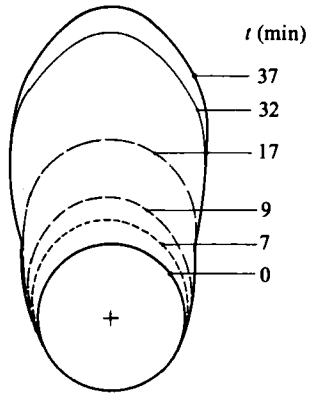

FIGURE 5. Interface shape and motion with respect to the heat source.

for the initially embedded case (figure 5). For $\phi < 90°$, the heat source 'saw' a fixed interface shortly after the experiment started ($t \geqslant 7$ min), and it may be concluded that a quasi-steady state has been reached for this portion of the interface. But, for $\phi > 90°$, such a conclusion is not valid as the interface is still moving with respect to the heat source. The height of the melt pool above the heat source is indeed a function of the imposed heat flux and also the initial temperature of the solid. The experimental setup permitted a maximum travel distance of 15 cm for the heat source. This was not enough for the interface to attain its quasi-steady-state shape with respect to the heat source in any of the experiments studied with a minimum heat flux of 1315 W/m^2 and maximum subcooling of 18°. Further reduction in the surface heat flux and/or increase in the subcooling of the solid was not attempted as side effects (i.e. solidification of the melt on the glass windows, mist formation on the outer glass plate and increase in the frictional force between the support tubes and the resolidified material) were expected to interfere with the experiments.

3.2. *Heat-source velocity*

In order to determine the velocity of the heat source, the instantaneous position of its centre was first plotted against time and smoothed by curve-fitting. The curve was then differentiated graphically to determine the heat-source velocity. Figure 6 illustrates the variation with time of the heat-source velocity for different surface-heat fluxes of the source while the solid temperature and the mass of the source were kept constant ($T_\infty = 21$ °C and $M = 275$ g). For all cases, the heat-source velocity attained its constant terminal value after first reaching a maximum. The solid symbols in the figure denote the times when the heat source was fully covered with the melt. The terminal velocity of the source was attained after it was completely covered by the melt. This indicates the effect of the convective cooling of the melt on the motion of the source. However, as already stated, the source velocity was defined at $\phi = 0°$ where the melt thickness is minimum and conduction is the dominant heat-transfer mechanism between the source and the solid. Therefore the uniformity of the heat flux at the surface of the source may be questioned.

In order to determine the relevant parameters that could be used to scale the data, an energy balance was made on the infinitesimal control volume at the lower stagnation point ($\phi = 0°$) and bounded by the source and the solid. Under a

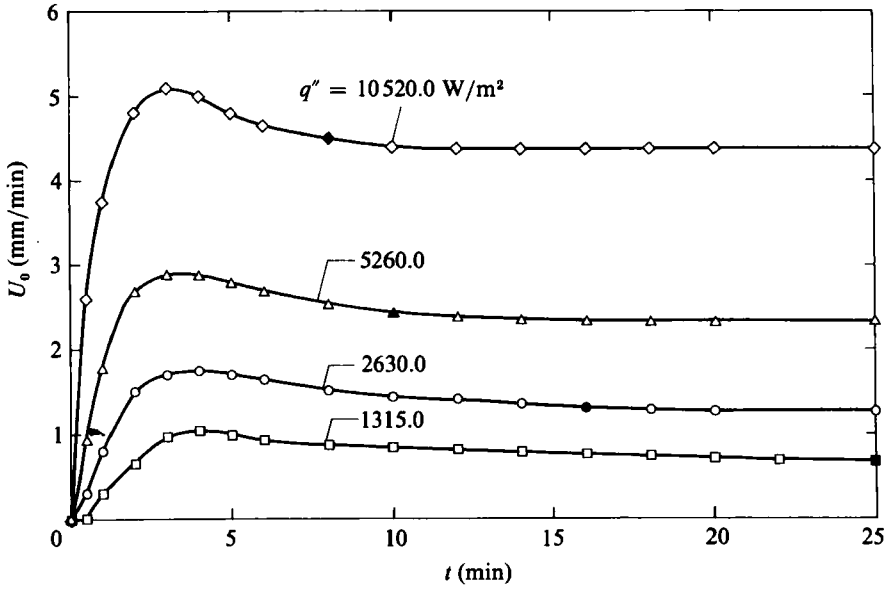

FIGURE 6. Variation of the heat-source velocity with time.

quasi-steady-state condition, the total heat input rate to the control volume per unit length is equal to $q''R\,\mathrm{d}\phi$ and is related to the heat-source velocity by

$$q''(R\,\mathrm{d}\phi) = \rho_s U_0[h_m + c_s(T_m - T_\infty)]\,(R\,\mathrm{d}\phi), \tag{1}$$

where U_0, R and q'' are the velocity, radius and surface-heat flux of the source, respectively; ρ_s, c_s and h_m are density, specific heat and latent heat of fusion of the solid; and T_∞ is temperature of the solid far from the heat source. In writing the above equation it was assumed that the melt leaves the control volume at the fusion temperature T_m and that the effect of cylindrical geometry on heat transfer to the solid is negligible. Both of these assumptions are well justified for a small enough angular increment $\mathrm{d}\phi$ and both result in an overestimation of U_0. Equation (1) can be rearranged to yield

$$\frac{U_0^*}{Ste} = 1 \tag{2}$$

where

$$U_0^* = U_0 R/\alpha,$$

α is thermal diffusivity of the melt, and $Ste = Rq''/[h_m + c_s(T_m - T_\infty)]$.

Figure 7 presents the variation of the dimensionless heat-source velocity (scaled by the Stefan number) as a function of dimensionless time, $Fo = \alpha t/R^2$, with the Stefan number as a parameter. The terminal value of the dimensionless velocity is well above the expected upper bound of unity suggested by (2). The physics of the problem rule out any heat transfer toward the lower stagnation point via the melt (to justify the source velocity exceeding its upper bound). Therefore, in spite of the careful consideration given to the heat-source design, some heat was conducted in the source in the circumferential direction toward the lower stagnation point where heat extraction from the heat source is much more intense than anywhere else.

An energy balance was made on the control volume bounded by the lower half ($-\frac{1}{2}\pi \leqslant \phi \leqslant \frac{1}{2}\pi$) of the heat source and the solid. The heat-transfer rate per unit

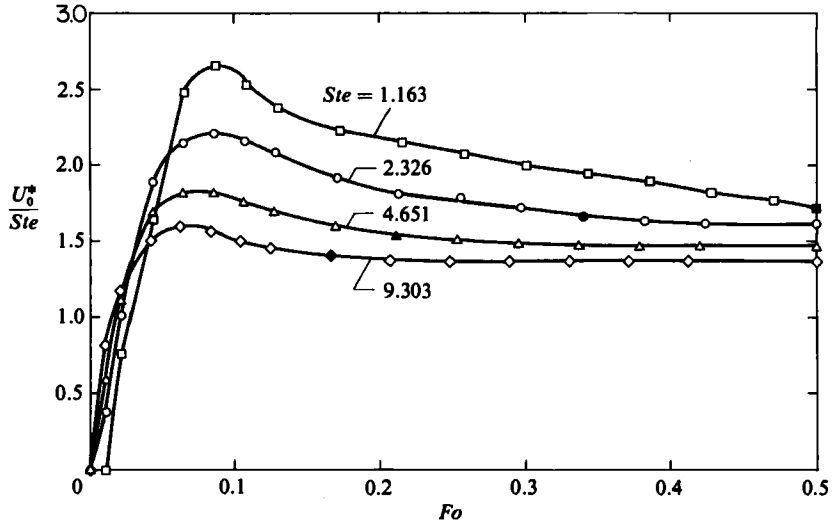

FIGURE 7. Variation of dimensionless heat-source velocity with dimensionless time.

length of the heat source to the melt film is $\pi Rq''$, and the rate is related to the heat-source velocity by

$$\pi Rq'' = \rho_s U_0(2R)[h_m + c_s(T_m - T_\infty)]. \tag{3}$$

In writing this equation it was again assumed that the melt leaves the control volume at the fusion temperature and the effect of cylindrical geometry on the rate of heat transfer to the solid is negligible (both resulting in an overestimation of U_0). Equation (3) may be rearranged to yield

$$\frac{U_0^*}{Ste} \leqslant \tfrac{1}{2}\pi = 1.57. \tag{4}$$

The estimated upper bound for U_0^*/Ste is in better agreement with results presented in figure 7. This suggests that, owing to the large variation of the heat-transfer coefficient around the heat source, an averaged analysis predicts realistic velocities for the heat source. Moreover, heat transfer from the upper half of the heat source to the lower half is of the same order of magnitude as the heat transferred to the melt as it is squeezed through the film channel. It should be noted here that the heat loss from the source to the glass walls is expected to have caused some non-uniformity in the melt-layer thickness under the heat source along its length (i.e. the melt layer being thinner near the glass walls). However, as the source velocity is defined by the point on the interface closest to the source, the three-dimensionality only reduced the source velocity.

The effect of the heat-source mass on its velocity was determined by varying its mass between 75 and 675 g (corresponding to $0.67 \leqslant \Delta\rho/\rho \leqslant 15.1$, where $\Delta\rho = \rho_{HS} - \rho$ and ρ_{HS} and ρ are densities of the heat source and melt respectively) while the surface heat flux and the initial temperature of the solid were kept constant ($q'' = 2630$ W/m^2, $T_\infty = 27.5$ °C, $Ste = 2.46$). The results proved that the heat-source velocity is not a function of the heat-source mass under these conditions. This is due to the fact that the rate of heat input to the source is constant, and increasing the mass of the source beyond the minimum required to initiate its motion will not decrease the thermal resistance between the source and the solid because of the finite thickness of the melt film.

It was also expected that reduction of the mass of the source below a certain minimum should be accompanied by a decrease in the terminal velocity of the heat source. A reduction in the source mass may cause an increase in the thermal resistance of the contact point and probably an increase in the thickness of the film layer between the heat source and solid. This could not be proven conclusively for two reasons. First, this minimum mass was very close to M_f (mass of the paraffin wax with the same volume as the heat source), and, secondly, the uncertainty associated with the force exerted by the heat source on the solid was of the same order of magnitude as M_f ($M_f = 45$ g compared to ± 15 g uncertainty). Such high uncertainty was due to continuous (in time) and inconsistent (in magnitude) interference of the supply lines of the heat source and also the change in frictional resistance between the bushings and the support tubes from one setting to another as well as during an experiment.

3.3. *Overshoot of heat-source velocity*

The effect of the thermal transients inside the heat source may be observed in figures 6 and 7, where the surface-heat flux is changed while the mass of the source, its initial temperature and its starting position (on the top of the solid) are kept constant. The time at which the maximum source velocity occurs increases slightly with a decrease in the surface-heat flux. This is owing to the fact that both the solid and the heat source were initially at 21 °C. The heating of the source and the solid to the fusion temperature causes a time lag in the initiation of melting, which increases with a reduction in the surface heat flux. The overshoot in the heat-source velocity may be inferred to be the result of coupling of the following transients: (1) development of a steady-state condition in the heat source; (2) development of a quasi-steady state in the melt film separating the heat source and the solid; (3) development of a quasi-steady state in the melt above the heat source, and (4) development of a quasi-steady-temperature field in the solid ahead of the heat source.

The heat-source velocity always reached its final constant value after it was covered by the melt (solid symbols in figures 6 and 7). This suggests that the heat extracted from the source by the melt had a stabilizing effect on the thermal development of the source. The finding was further verified in experiments where the effect of the melt was eliminated partly (by removing the melt above $\phi = 90°$ with a syringe at 30 s intervals during the test) or entirely (by removing the confining glass walls so that the melt would run off). The dependence of the heat-source velocity on time for these experiments are compared with the experiments where no melt was removed (figure 8). These results confirm the stabilizing effect of the melt motion on the thermal development of the heat source and also suggest that the heat extracted by the melt is greatest underneath the heat source since the removal of melt above $\phi = 90°$ did not change the overall characteristics of the source-velocity variation with time. The partial melt removal (above $\phi = 90°$) resulted in an increase of about 10 % in the terminal velocity, while complete melt removal caused an increase of about 42 %. When melt removal was terminated (at $t = 28$ min), the source velocity decreased and reached the terminal value for the experiment in which no melt was removed as soon as the source was covered by the melt.

The effect of the initial position of the heat source on its velocity is also shown in figure 8. When the heat source was initially embedded in the solid the convection in the melt is more vigorous, especially at the early stages, when compared with the experiment when the source was initially on the top of the solid. As melting proceeds and the source descends, the effect of the top surface boundary for either case (solid

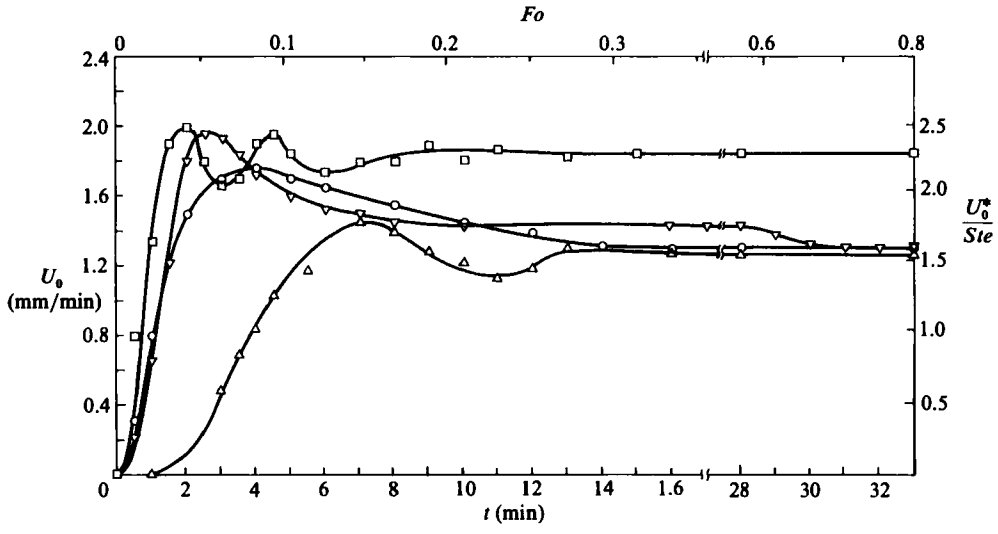

FIGURE 8. Variation of the heat-source velocity with time: ○, heat source initially on top of the solid; □, heat source initially on top of the unconfined solid; ▽, heat source initially on top of the solid and melt above $\phi = 90°$ removed during the experiment; △, heat source initially embedded in the solid, $Ste = 2.326$ and $T_\infty = 23$ °C.

ceiling of free surface) gradually vanishes, and the cooling effect of the melt on the heat source becomes similar as revealed by the flow patterns. The terminal velocity of the embedded source is only about 5 % smaller than that of the experiment in which the heat source was on the top of the solid initially. This may be attributed to the higher friction on the support tubes in the experiments when the source was embedded.

The effect of thermal development of the heat source on its descent velocity may also be inferred from figure 9, where variation of dimensionless temperature of the source, $(T_w - T_m)\,k/(q''R)$, with the dimensionless time (Fo) is presented for three different angular positions ϕ on the source. Like the descent velocity of the source, the heat-source surface temperature experiences an overshoot. As the source was initially at a temperature equal to the solid temperature, and more than a single heat-transfer mechanism is involved (internal circumferential heat conduction and external cooling effect of melt) it is reasonable to expect an overshoot in the surface temperature of the source. Comparison of figures 7 and 9 reveals that the maximum temperature on the source at $\phi = 0°$ occurred before the heat source reached its maximum velocity. This indicates that the overshoot in the source velocity is indeed a consequence of the heat source undergoing thermal transience. The overshoot of the temperature for $\phi = 0°$ is much smaller and occurs sooner than those corresponding to $\phi = 90°$ and 180°. The findings support the conclusion made earlier that close to the lower stagnation point conduction is the only mechanism for heat transfer.

The solid symbols in figure 9 represent the times at which the corresponding thermocouple (at 90° or 180°) was covered with the melt. The thermocouple at $\phi = 90°$ does not attain its constant final value until the heat source is completely covered by the melt. However, the thermal development of the heat source may be considered to be completed only 4 minutes after it was fully covered by the melt. In other words, with the terminal source velocity of 1.3 mm/min in this case, the temperature field on the heat source became fully developed only after it was covered by 8 mm of melt

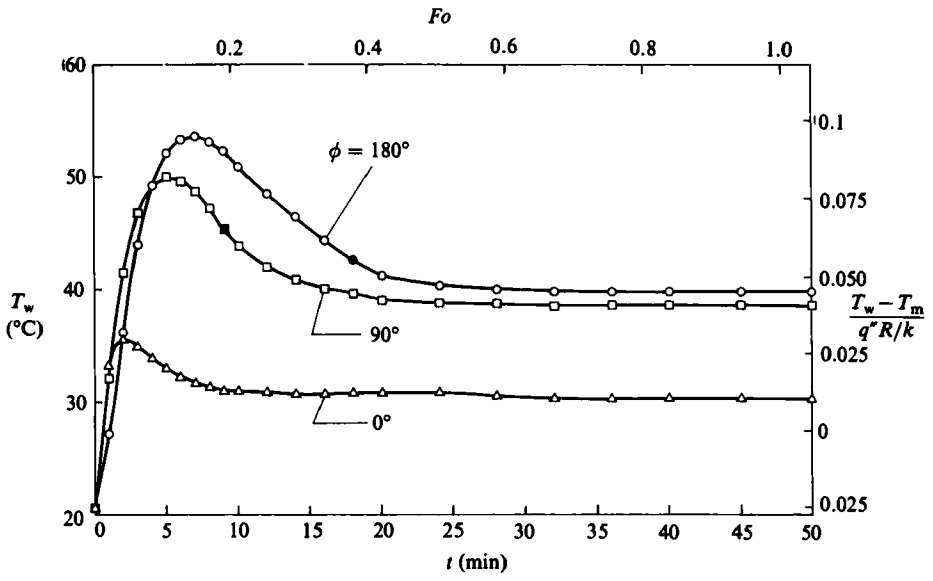

FIGURE 9. Variation of heat-source surface temperatures with time, $q'' = 2630$ W/m^2, $T_\infty = 21$ °C ($Ste = 2.326$).

or 50 % of the radius of the source. The temperature rise at $\phi = 180°$ lagged that at $\phi = 0°$ and 90° at early times. This is due to the fact that the patch heater did not cover the entire circumference of the inner cylinder (due to the gap left to allow for expansion during heating), and its ends were 3 mm apart at $\phi = 180°$ to provide passage for the thermocouple wires and electric leads of the heater to the outer cylinder and support tubes. Thus no heat was generated between $\phi = 174°$ and 186°, which resulted in a delay in temperature rise at $\phi = 180$ °C.

3.4. *Temperature in the solid and liquid*

The temperature distribution in the melt was measured by placing a probe consisting of five thermocouples above the heat source (z-axis). Figure 10 (on the right) shows the temperature distribution in the melt at different vertical positions with respect to the heat source. The temperatures are uniform in the middle portion of the melt pool. Away from the heat source this flatness extends towards the centreline, while remaining steep close to the solid–liquid interface. These trends are in agreement with the flow-visualization observations which suggested a region of stagnant melt in the middle of the melt pool on either side of the heat source. The uniformity of the temperatures over the melt region also suggests a reduction of the buoyancy force near the centreline as the melt moves away from the heat source. Regardless of the fact that (for an initially subcooled solid) cooling of the melt eventually causes its resolidification on the vertical solid walls (and the solid ceiling in the embedded case), this process is so slow that an observer on the heat source (and moving with it) sees a quasi-steady temperature in the melt pool. This point was discussed earlier and was also examined by changing the position of the thermocouple probe in the melt. The thermocouple readings were found to be independent of the position of the probe in the melt (with respect to laboratory fixed coordinates) but were a function of the distance between the probe and the heat source. The result suggests that the melt has reached a quasi-steady state with respect to the descending heat source. This conclusion permitted plotting the temperature contours in the melt by connecting

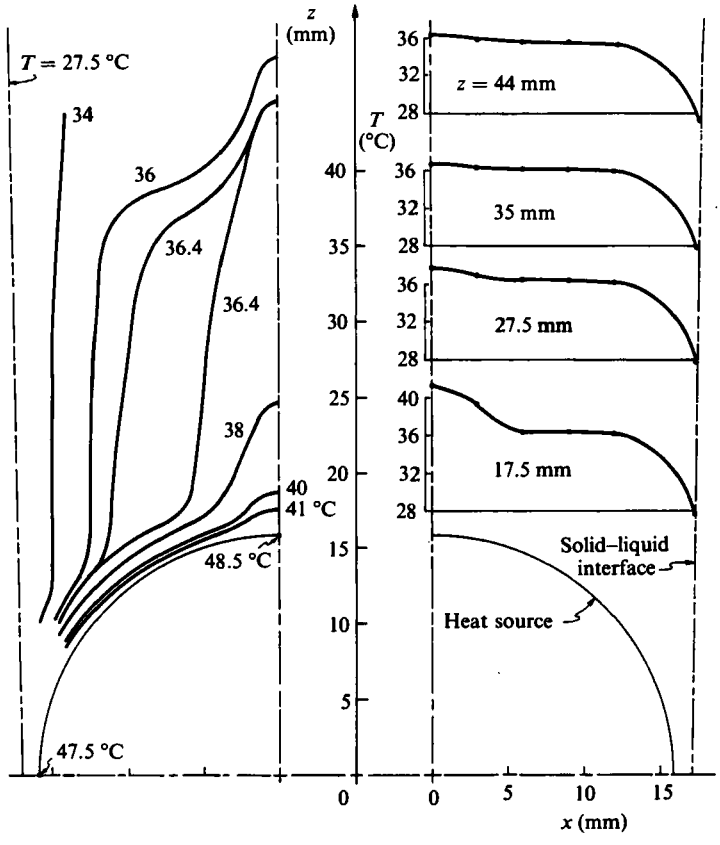

FIGURE 10. Temperature isotherms in the liquid (on the left) and temperature distributions in the melt at different positions relative to the heat source (on the right), $q'' = 5260$ W/m^2 and $T_\infty = 21$ °C.

points of equal temperature (figure 10, on the left). The isotherms show a region of constant temperature (and stagnant fluid) in the melt pool. The closely spaced isotherms near the heat source indicate a region of a large temperature gradient near the heat-source surface. This is in agreement with the flow-visualization observations which showed that the newly melted material formed a boundary layer on the heat source when squeezed out between the source and the solid–liquid interface.

Figure 11 (on the right) shows the temperature profiles in the solid at different times and vertical positions with respect to the source. Two racks of thermocouples which were positioned vertically in the solid 30 mm apart recorded the same temperatures when they were at the same distance from the heat source. This confirmed that the solid and the melt had reached the quasi-steady state with respect to the heat source. The finding is at least true for the solid ahead of the source and in its vicinity where the solid–liquid interface has already reached the quasi-steady-state shape. The isotherms in the solid are plotted by connecting points of equal temperature and are also presented in figure 11 (on the left). The contour lines are most closely spaced in front of the source where heat transfer to the solid is at its highest rate (i.e. the liquid film is the thinnest). Above and away from the heat source, the isotherms start to become parallel to each other and are more evenly spaced. This is another indication that the interface in this region is far from its quasi-steady-state shape.

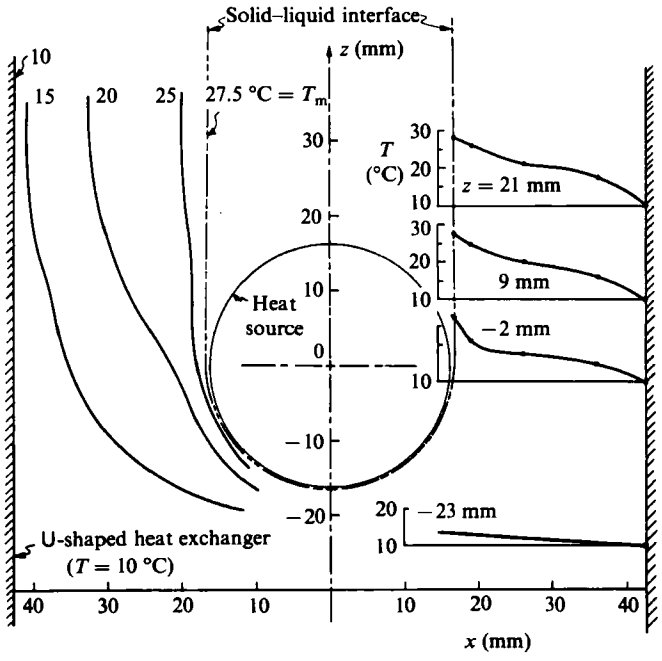

FIGURE 11. Temperature isotherms (on the left) and temperature distributions in the solid at different positions relative to the heat source (on the right), $q'' = 2630$ W/m^2 and $T_\infty = 10$ °C.

4. Conclusions

The experiments performed have provided phenomenological understanding and also quantitative data on flow and melting around a migrating horizontal, cylindrical heat source. Important heat-transfer mechanisms were identified, and the domain, extent and duration of their influence were investigated.

Conduction was found to be the dominant heat-transfer mechanism around the lower stagnation point of the source, where the heat source and the solid are in almost permanent contact for the range of parameters investigated ($0.67 \leqslant \Delta\rho/\rho \leqslant 15.1$ and $1.23 \leqslant Ste \leqslant 9.84$). Large variation of the heat-transfer coefficient around the heat source resulted in some heat conduction in the body of the source in the circumferential direction towards the lower stagnation point. As a consequence, the experimental results did not agree with the predictions (based on uniform surface heat flux). Terminal heat-source velocity determined from an energy balance on the lower half of the source was found to be in better agreement with the experimental results.

The convective heat transfer to the melt along the film channel was found to dampen the thermal development of the heat source and in a sense accelerate the stabilization of the temperature field on the heat source. The fluid motion in the melt pool above the heat source was mainly induced by the descent of the source, while natural convection played only a minor role in this motion.

The heat source and the solid–liquid interface in its immediate vicinity reached their quasi-steady conditions at the same time. This also coincided with the completion of the boundary-layer formation of the newly melted material on and over the heat source. However, the solid–liquid interface away from the heat source and also the melt pool above the source (outside of the boundary layer) needed much more time to reach their quasi-steady state with respect to the heat source. This was

concluded to be a result of weak interaction between the heat source and the melt pool due to the formation of the boundary layer over the heat source.

The work reported in this paper was supported, in part, by the National Science Foundation Heat Transfer Program under Grant No. MEA-8313573.

REFERENCES

ARMSTRONG, D. E., COLEMAN, J. S., MCINTEER, B. B., POTTER, R. M. & ROBINSON, E. S. 1965 Rock melting as a drilling technique. *Report* LA-3243, Los Alamos Scientific Laboratory.

CHRISTOFFEL, D. A. & CALHAEN, I. M. 1973 Upper mantle viscosity determined from Stokes' Law. *Nature Phys. Sci.* **243**, 51–52.

COHEN, J. J., SCHWARTZ, L. L. & TEWES, H. A. 1974 Economic and environmental evaluation of nuclear waste disposal by underground *situ* melting. *Am. Nuc. Soc. Trans.* **18**, 194–195.

DONEA, J. 1972 Operation hot mole. *Euro-Spectra* **11**, 102–109.

EASTON, C. R. 1968 Conduction from a finite-size moving heat source applied to radioisotope capsule self-burial. *N.B.S. Special Publication* 302, pp. 209–2188.

EMERMAN, S. H. & TURCOTTE, D. L. 1983 Stokes's problem with melting. *Intl J. Heat Mass Transfer* **26**, 1625–1630.

HARDEE, H. C. & SULLIVAN, W. N. 1973 Waste heat melt problem. *Report* SLA-73-0575, Sandia Lab. Albuquerque, New Mexico.

HARDEE, H. C. & SULLIVAN, W. N. 1974 An approximate solution for self-burial rates of radioactive waste containers. *Report* SL-73-0931, Sandia Laboratories, Albuquerque, New Mexico.

HERRMANN, A. G. 1983 *Radioaktive Abfälle.* Springer.

JACKSON, F. 1965 Moving heat sources with change of phase. *Trans. ASME* C: *J. Heat Transfer* **87**, 329–332.

JANSEN, G. & STEPNEWSKI, D. D. 1973 Fast reactor fuel interactions with floor material after a hypothetical core melt-down. *Nucl. Techn.* **17**, 85–96.

LOGAN, S. E. 1974 Deep self-burial of radioactive wastes by rock-melting capsules. *Nucl. Techn.* **21**, 111–124.

MARSH, B. D. 1978 On the cooling of ascending andesitic magma. *Phil. Trans. R. Soc. Lond.* A **288**, 611–625.

MARSH, B. D. & CHARMICHAEL, I. S. E. 1974 Benioff zone magnetism. *J. Geophys. Res.* **79**, 1196–1206, 32–46.

RASMUSSEN, N. C., YELLIN, J., KLEITMAN, D. J. & STEWART, R. B. 1979 Nuclear power: Can we live with it? *Tech. Rev.* 81,

ROBINSON, E. S., POTTER, R. M., MCINTEER, B. B., ROWLEY, J. C., ARMSTRONG, D. E., MILLS, R. L. & SMITH, M. C. 1971 A preliminary study of the nuclear subterrene. *Report* LA-4547, Los Alamos Scientific Laboratory.

TONG, L. S. 1968 Core cooling in a hypothetical loss of coolant accident. Estimate of heat transfer in core meltdown. *Nucl. Engng Design* **88**, 309–312.